

Uncertainty Quantification in Volumetric PTV

Sayantana Bhattacharya^{1*}, Pavlos P. Vlachos¹

¹Purdue University, Department of Mechanical Engineering, West Lafayette, USA

*bhattach3@purdue.edu

Abstract

We introduce the first comprehensive approach to determine the uncertainty in a volumetric Particle Tracking Velocimetry (PTV) measurement. Volumetric PTV is a state-of-the-art non-invasive flow measurement technique, which measures the velocity field by recording successive snapshots of the tracer particle motion using a multi-camera set-up. The measurement chain involves reconstructing the three-dimensional particle positions by triangulation process using the calibrated camera mapping functions. The non-linear combination of the elemental error sources during the different steps of the process further enhances the complexity of the task. Here, we first estimate the uncertainty in the particle image location, which we model as a combination of the particle position estimation uncertainty and the reprojection error uncertainty. The latter is obtained by a gaussian fit to the histogram of disparity estimates within a sub-volume. Next, we determine the uncertainty in the camera calibration coefficients. As a final step the previous two uncertainties are combined using an uncertainty propagation through the volumetric reconstruction process. The uncertainty in the velocity vector is directly obtained as a function of the reconstructed particle position uncertainty. The framework is tested with synthetic vortex ring images. The results show good agreement between the predicted and the expected RMS uncertainty values. The prediction is consistent for seeding densities tested in the range of 0.01 to 0.1 particles per pixel. Finally, the methodology is also successfully validated for an experimental test case with laminar pipe flow velocity profile measurement.

Nomenclature

x_w, y_w, z_w : World coordinates or physical coordinates

X^c, Y^c : Camera image coordinates for camera c

FX^c, FY^c : X and Y calibration mapping function for camera c

a_i : camera mapping function coefficients

e : Error in any variable

σ : Standard uncertainty in any variable

Σ : Full covariance matrix for any variable

\vec{d} : Disparity vector estimated from ensemble of reprojection error.

u, v, w : Velocity components in x, y, z directions respectively.

1 Introduction

Volumetric PTV (Baek & Lee 1996; Maas *et al.* 1993; Ohmi & Li 2000; Pereira *et al.* 2006) is a fluid velocity measurement technique which resolves the three-dimensional (3D) flow structures by tracking the motion of tracer particles introduced in the flow. The tracer particle motion is recorded with multiple cameras to obtain projected particle images. Each camera is also linked to the physical space using a calibration mapping function (Soloff *et al.* 1997). The particle images are then mapped back to the physical space using a triangulation process (Maas *et al.* 1993; Wieneke 2008). Finally, a three-dimensional (3D) tracking of the reconstructed particles estimates the Lagrangian trajectories of the particles and subsequently resolves the volumetric velocity field. PTV easily lends itself to calculation of particle acceleration from the tracked trajectories. Also, unlike Tomographic Particle Image Velocimetry (Tomo-PIV) (Elsinga *et al.* 2006), which involves spatial averaging over the interrogation window, 3D PTV has higher spatial resolution as it yields a vector for every tracked particle position. However, there is a tradeoff in terms of the number of particles as for higher seeding density the error in reconstruction as well as particle pairing increases. Hence, the simple triangulation based 3D PTV method introduced in 1993 (Maas *et al.* 1993) had limited applications compared to Tomo-PIV for highly seeded flows. Improvements in terms of particle identification (Cardwell *et al.* 2011) and tracking algorithms (Cowen *et al.* 1997; Fuchs *et al.* 2016, 2017; Lei *et al.* 2012; Riethmuller 2001; Takehara *et al.* 2000) have been proposed to minimize the error in the measurement.

Recent advancements in terms of reconstruction algorithms, such as Iterative Particle Reconstruction (IPR) (Wieneke 2013) and Shake-the-box (STB) (Schanz *et al.* 2016) have significantly improved the accuracy of 3D PTV. IPR uses an initial triangulation based reconstructed field to construct a projected image and then minimizes the intensity residuals in the image plane by shaking the particles world coordinate location. This process achieves a better positional accuracy, reduced fraction of ghost particles and the accuracy is comparable to MART (Multiplicative Algebraic Reconstruction Technique) (Elsinga *et al.* 2006) up to a seeding density of 0.05 particles per pixels (ppp). This concept has been further advanced in STB, which uses the temporal information, for a time-resolved measurement, to predict the particle location in the future frames and corrects the predicted position iteratively using IPR. Such measurements have successfully resolved flow structures for experiments with high particle concentrations (up to 0.125 ppp). With such capabilities, 3D PTV measurements have gained renewed attention and applicability in various experiments.

To analyze any experimental results with statistical significance, uncertainty quantification (UQ) is crucial, especially, where the measured data are used in a design process or to validate computational models. Given the increasing applicability and relevance of PTV/IPR/STB volumetric measurements, providing uncertainty estimation for an individual 3D PTV measurement is now critical.

Uncertainty estimation in non-invasive PIV measurements has received interest only recently and several methods have been proposed for planar PIV uncertainty quantification. Broadly such methods can be categorized into direct and indirect methods. Indirect methods rely on a calibration function, which maps an estimated measurement metric (e.g. correlation plane signal to noise ratio metrics (Charonko & Vlachos 2013; Xue *et al.* 2014, 2015) or estimates of the fundamental sources of error (Timmins *et al.* 2012)) to the desired uncertainty values. Such a calibration is developed from a simulated image database and may not be sensitive to a specific error source for a given experiment. Direct methods, on the other hand, rely directly on the measured displacements and use the image plane “disparity” (Sciacchitano *et al.* 2013; Wieneke 2015) information or correlation-plane PDF (probability density function) of displacement information (Bhattacharya *et al.* 2018) to

estimate the a-posterior uncertainty values. Comparative assessments(Boomsma *et al.* 2016; Sciacchitano *et al.* 2015) have shown that the direct methods are more sensitive to the random error sources. However, indirect methods can be potentially used to predict any bias uncertainty. An uncertainty estimation for stereo-PIV measurement(Bhattacharya *et al.* 2017) has also been proposed recently. A detailed review of such methods can be found in (Sciacchitano 2019). Thus, although the foundations have been laid for planar and stereo-PIV uncertainty quantification, applicability of such methods to 3D measurements remains untested and these methods train strictly to cross-correlation based measurements. As a result, 3D reconstruction and tracking process for 3D PTV measurements is not covered under these methods and currently a-posterior uncertainty quantification methods for volumetric measurements (PTV/PIV) does not exist and new uncertainty model development is needed.

A schematic for the different steps in a 3D PTV measurement chain is shown in Figure 1. The first step establishes a mapping function between the camera image coordinates(X, Y) and the world coordinates(x_w, y_w, z_w) in the physical space using a multi-camera calibration process. The calibration coefficients are then iteratively corrected using the mapping function and the recorded particle images to eliminate any misalignment between the assumed world coordinate system origin of the calibration plane and the actual origin location for the measurement volume. This process is called volumetric self-calibration(Wieneke 2008) and is essential in minimizing the

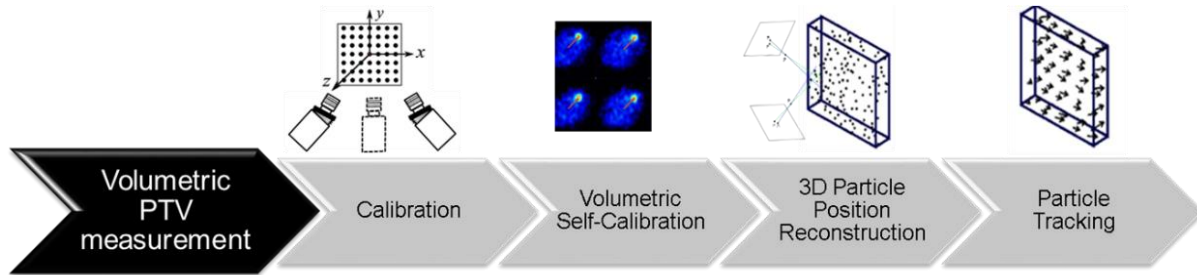


Figure 1: A volumetric PTV measurement chain showing the main steps in the process.

reconstruction error (due to existing offset or disparity between cameras) and improving the calibration accuracy. Using the modified calibration, for each particle in a given camera, the corresponding match in the second camera is searched along the epipolar line and the particle matches in all cameras are triangulated(Maas *et al.* 1993; Wieneke 2008) to a world position. This can be done in an iterative sense for an IPR type algorithm. The reconstruction process solves the inverse problem using an underdetermined system of equations and is one of the main sources of error in the process. Finally, the reconstructed 3D particle positions are tracked to find the velocity vectors using “nearest neighbor” or other advanced algorithms(Fuchs *et al.* 2017). The tracking and reconstruction can be done in conjunction for STB type evaluations. From calibration fitting error, particle position estimation error, the disparity vector estimation error to the error in finding the 3D positions and its pairing, the errors in each step of the process are inter-linked in a complex non-linear way and affect the overall error propagation. The iterative corrections and the governing non-linear functions lead to several interdependent error sources making the definition of a data reduction equation intractable and the development of an uncertainty quantification model non-trivial.

In the current framework, a model is developed to quantify the uncertainty in particle image position and the mapping function coefficient. These uncertainties are in turn combined with the uncertainty propagation through the reconstruction process. Finally, the uncertainty in the velocity vector is expressed directly as a combination of the position uncertainty in the matching pair of particles. The methodology is described in detail in the next section.

2 Methodology

The primary relation between the observed image coordinate (X, Y) and the expected particle world coordinate (x_w, y_w, z_w) in physical space is given by the individual camera mapping function FX^c for each camera c , as given in equation (1).

$$\begin{aligned} X^c = FX^c(x_w, y_w, z_w, a_i) = & a_1 + a_2x_w + a_3y + a_4z + a_5x_w^2 + a_6x_wy_w + a_7y_w^2 \\ & + a_8x_wz_w + a_9y_wz_w + a_{10}z_w^2 + a_{11}x_w^3 + a_{12}x_w^2y_w + a_{13}x_wy_w^2 \\ & + a_{14}y_w^3 + a_{15}x_w^2z_w + a_{16}x_wy_wz_w + a_{17}y_w^2z_w + a_{18}x_wz_w^2 + a_{19}y_wz_w^2 \end{aligned} \quad (1)$$

Typically, a polynomial mapping function is used following Soloff et al. (Soloff *et al.* 1997) to have higher accuracies in the presence of optical distortion effects. Once a mapping function is established and iteratively corrected using self-calibration process, the reconstruction process involves finding an inverse of the mapping function for the matching particle image coordinates in different projections. Hence an error propagation through the mapping function is the starting point of the uncertainty quantification and is described in the next subsection.

Error propagation through the mapping function

An error propagation for equation (1) can be written as follows:

$$e_{X^c} = \frac{\partial FX^c}{\partial x_w} e_{x_w} + \frac{\partial FX^c}{\partial y_w} e_{y_w} + \frac{\partial FX^c}{\partial z_w} e_{z_w} + \frac{\partial FX^c}{\partial a_i} e_{a_i} \quad (2)$$

Equation (2) is obtained as a Taylor series expansion of equation (1), neglecting the higher order terms. Thus, the error in image coordinate e_{X^c} can be related to the error in world coordinate positions e_{x_w} , e_{y_w} , e_{z_w} and the error in calibration function coefficients e_{a_i} through the mapping function gradients $\left(\frac{\partial FX^c}{\partial x_w}, \frac{\partial FX^c}{\partial y_w}, \frac{\partial FX^c}{\partial z_w}, \frac{\partial FX^c}{\partial a_i}\right)$. A similar propagation equation can be written for the error in Y (e_{Y^c}) image coordinate for each camera mapping function. It is important to note that the quantities of interest are e_{x_w} , e_{y_w} , e_{z_w} as we seek to estimate the unknown variance in the reconstructed world coordinate positions. Rearranging the unknown terms in the left-hand side and multiplying each side by its transpose yields the variance propagation equation as follows:

$$\begin{aligned} & \left(\frac{\partial FX^c}{\partial x_w} e_{x_w} + \frac{\partial FX^c}{\partial y_w} e_{y_w} + \frac{\partial FX^c}{\partial z_w} e_{z_w}\right) \left(\frac{\partial FX^c}{\partial x_w} e_{x_w} + \frac{\partial FX^c}{\partial y_w} e_{y_w} + \frac{\partial FX^c}{\partial z_w} e_{z_w}\right)^T \\ & = \left(e_{X^c} - \frac{\partial FX^c}{\partial a_i} e_{a_i}\right) \left(e_{X^c} - \frac{\partial FX^c}{\partial a_i} e_{a_i}\right)^T \end{aligned} \quad (3)$$

Assuming that e_{X^c} and e_{a_i} are independent, a more simplified version of equation (3) can be written as shown in equation (4).

$$C_{\vec{x}_w} \Sigma_{\vec{x}_w} C_{\vec{x}_w}^T = \Sigma_{\vec{X}} + C_{\vec{a}} \Sigma_{\vec{a}} C_{\vec{a}}^T \quad (4)$$

Here, $C_{\vec{x}_w}$ represents the coefficient matrix containing mapping function gradients with respect to $\vec{x}_w = \{x_w, y_w, z_w\}$ and $C_{\vec{a}}$ represents the mapping function gradients with respect to the coefficients a_i . This equation can be written as a stack of 8 rows of equations corresponding to X and Y mapping functions for each of, for example a four-camera set-up. In this case $\Sigma_{\vec{X}}$ would represent a diagonal matrix with the diagonal entries containing the uncertainty in particle image position estimation for each projection. Equation (4) contains the unknown covariance matrix in world coordinates ($\Sigma_{\vec{x}_w}$) as a function of $\Sigma_{\vec{X}}$ and $\Sigma_{\vec{a}}$. The following sections focus on estimating the $\Sigma_{\vec{X}}$ and $\Sigma_{\vec{a}}$ terms.

The overview of the uncertainty estimation and propagation process is depicted in Figure 2.

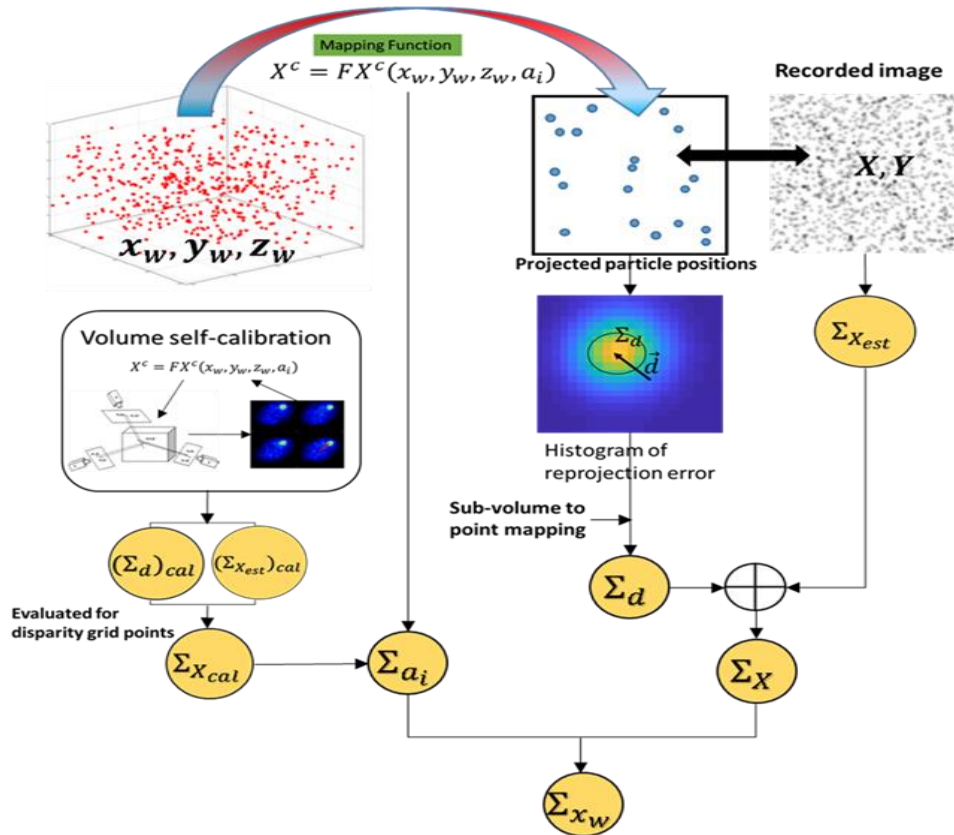


Figure 2: A schematic showing different steps for estimating elemental uncertainties in particle image location X and calibration coefficients a_i and its propagation to the uncertainty in the world coordinate x_w .

Estimating uncertainty in particle image location

For a-posteriori uncertainty quantification, we start from a reconstructed 3D particle positions obtained either from a triangulation or IPR reconstruction method. For a given 3D particle position,

we want to find the corresponding projected particle image locations and its uncertainty for each camera. As shown in Figure 2, the projected particle positions are compared with the recorded image to find the error in particle image location. This can be expressed as a sum of the estimated projection error ($\vec{X}_{proj} - \vec{X}_{est}$) and the 2D particle fit position estimation error ($\vec{X}_{est} - \vec{X}_{true}$), as shown in equation (5).

$$e_{\vec{x}} = \vec{X}_{proj} - \vec{X}_{true} = \vec{X}_{proj} - \vec{X}_{est} + \vec{X}_{est} - \vec{X}_{true} \quad (5)$$

Thus, the variance in particle image location, $\Sigma_{\vec{x}}$, becomes a sum of the variance in the estimated projection error, denoted by $\Sigma_{\vec{d}}$, and variance of the error in particle image position estimation.

$$\Sigma_{\vec{x}} = e_{\vec{x}} e_{\vec{x}}^T = \Sigma_{\vec{d}} + \Sigma_{\vec{x}_{est}} \quad (6)$$

In order to estimate $\Sigma_{\vec{d}}$ the reconstruction domain is divided into subvolumes and the estimated projection error for a group of particles belonging to the same subvolume are stacked up into a histogram (this relates to the concept of disparity(\vec{d}) defined by Wieneke (Wieneke 2008)). The subvolume size can be varied or particles from other frames can be included to have a larger statistical sample. Such a histogram of disparity(\vec{d}) estimates is shown in Figure 2, where a mean disparity is shown along with a circle denoting the variance in the estimated projection error $\Sigma_{\vec{d}}$. For a perfectly converged self-calibration, the mean disparity should be zero. A gaussian fit is applied on this histogram and the estimated width is used to estimate the variance of the disparity distribution. In this framework, this estimated variance is modeled as the desired $\Sigma_{\vec{d}}$ of equation (6). For the particles belonging to the same subvolume, the same value of $\Sigma_{\vec{d}}$ is used.

$$\Sigma_{\vec{x}_{est}} = (J^T J)^{-1} \sigma_{res}^2 I \quad (7)$$

Each particle image within ± 0.5 pixels of the projected 3D particle location is fitted with a Gaussian shape and thus the uncertainty in the fitted position parameter for the least square fit process is considered as $\Sigma_{\vec{x}_{est}}$. Equation (7) denotes an expression for the position estimation variance which is shown to be a function of the variance in the fit residual error (σ_{res}^2) and the Jacobian(J) of the residual at the solution point (I denotes an identity matrix). Hence, once $\Sigma_{\vec{d}}$ and $\Sigma_{\vec{x}_{est}}$ are estimated the $\Sigma_{\vec{x}}$ is known.

Estimating the uncertainty in mapping function coefficients

As seen from the flowchart in Figure 2, once the variance in particle image position($\Sigma_{\vec{x}}$) is estimated through the progression of steps shown on the right side, the next workflow is focused on estimating the variance in the calibration coefficients ($\Sigma_{\vec{a}}$). This process can be performed in conjunction with the volumetric self-calibration process. If we consider the world coordinate positions ($x_{cal}, y_{cal}, z_{cal}$) where the disparity vectors are evaluated, then those grid points being specific locations in space, will have no uncertainty in their location. However, the presence of disparity between estimated and projected points leads to a shift in the projected grid points

(X_{cal}, Y_{cal}) in the image domain, this correction leads to a new set of coefficients (a_i) in the self-calibration process. Hence, the uncertainty in X_{cal}, Y_{cal} positions, namely $\Sigma_{\bar{x}_{cal}}$, should directly affect the $\Sigma_{\bar{a}}$. Consequently, the unknowns $(e_{x_w}, e_{y_w}, e_{z_w})$ of equation (3) can be simplified to zero and the equation can be simplified to equation (8).

$$\Sigma_{\bar{x}_{cal}} = \left(\frac{\partial FX}{\partial a_i} e_a \right) \left(\frac{\partial FX}{\partial a} e_{a_i} \right)^T = C_{\bar{a}} \Sigma_{\bar{a}} C_{\bar{a}}^T \quad (8)$$

In this equation, the $C_{\bar{a}}$ represents the gradients of the mapping function with respect to the coefficients a_i . The variance in the particle image position $\Sigma_{\bar{x}_{cal}}$ can be evaluated in a similar way as mentioned in section 0. Here, the $\Sigma_{\bar{x}_{cal}}$ can be evaluated for the initially triangulated particle positions and is used in equation (8) to solve for $\Sigma_{\bar{a}}$ as a least squares problem for all disparity grid points.

Uncertainty propagation in reconstructed positions

The uncertainty in the reconstructed world coordinate position is finally obtained by solving for the world coordinate location covariance matrix $\Sigma_{\bar{x}_w}$ from equation (4). This equation is evaluated for each world coordinate position for mapping functions in X and Y for all four cameras. The term $C_{\bar{a}} \Sigma_{\bar{a}} C_{\bar{a}}^T$ is evaluated using the estimated covariance $\Sigma_{\bar{a}}$. The $\Sigma_{\bar{x}}$ has already been calculated using equation (6). Hence, we solve for $\Sigma_{\bar{x}_w}$ by inverting the $C_{\bar{x}_w}$ matrix as shown in equation (9).

$$\Sigma_{\bar{x}_w} = B (\Sigma_{\bar{x}} + C_{\bar{a}} \Sigma_{\bar{a}} C_{\bar{a}}^T) B^{-1} \quad (9)$$

Where, B is given by $B = (C_{\bar{x}_w}^T C_{\bar{x}_w})^{-1} C_{\bar{x}_w}^T$. It can be noted that assuming no covariance between X and Y particle image position uncertainty, the term $(\Sigma_{\bar{x}} + C_{\bar{a}} \Sigma_{\bar{a}} C_{\bar{a}}^T)$ is essentially an 8x8 diagonal matrix for 8 mapping function equations. From the covariance matrix $\Sigma_{\bar{x}_w}$, the standard uncertainty in reconstructed positions $(\sigma_{x_w}, \sigma_{y_w}, \sigma_{z_w})$ are obtained by taking the square root of the diagonal terms $(\sqrt{(\Sigma_{\bar{x}_w})_{ii}})$.

Uncertainty in estimated velocity field

The uncertainty in each tracked 3D velocity measurement is evaluated as a direct combination of the estimated 3D position uncertainties of each paired particle. Thus, if a particle in frame 1 $(\sigma_{x_{w1}}, \sigma_{y_{w1}}, \sigma_{z_{w1}})$ is paired with a particle in frame 2, then the uncertainty in the tracked displacement σ_u is given by

$$\sigma_u^2 = \sigma_{x_{w1}}^2 + \sigma_{x_{w2}}^2 \quad (10)$$

The uncertainty in v and w components (σ_v, σ_w) can be obtained in a similar way following equation (10). It is to be noted, that the uncertainty due to false matching may need further analysis. However, for a valid measurement we expect equation (10) to account for the uncertainty in the tracked velocity measurement.

3 Results

The framework to estimate the uncertainty in the reconstructed particle positions is tested using synthetic vortex ring images. The particle field was generated and advected using incompressible axisymmetric vortex ring equations mentioned in (Wu *et al.* 2006). The camera calibration and particle images (256x256 pixels) were generated using in-house code. The camera angles were selected as 35° and were positioned in a plus(+) configuration. The volume of interest was set to 42mmx42mmx24mm and the seeding density was varied from 0.01ppp to 0.1ppp. The processing was also done using in-house calibration and IPR code. The initial estimate of the calibration was modified by the volumetric self-calibration to eliminate any mean disparity. An allowable triangulation error of 1 pixel was used for initial triangulation with dynamic particle segmentation method (Cardwell *et al.* 2011) to better resolve overlapping particle images. The particle image positions were estimated using least square Gaussian fit. The optical transfer function (OTF) (Schanz *et al.* 2013) was evaluated and used in IPR iterations. The number of inner loop and outer loop iterations for each frame was set to 4 and particle “shaking” of ± 0.1 pixels was used. The 3D particle tracking was done using “nearest neighbor” algorithm. The uncertainty for each measurement was computed using the set of equations described in section 2.

Comparing error and uncertainty histogram for reconstructed particle positions

First, the uncertainty in reconstructed particle positions are analyzed. The reconstructed particle positions are compared with the true particle positions in space and if a particle is found within 1 voxel radius of the true particle, then it is considered as a valid reconstruction. The error in reconstructed x_w position is denoted by e_{x_w} and defined as:

$$e_{x_w} = x_w^{estimated} - x_w^{true} \quad (11)$$

Similarly, e_{y_w} and e_{z_w} are defined. Figure 3 shows the histogram of error and uncertainty distributions x_w, y_w and z_w coordinates. Figure 3a and Figure 3b shows the distributions for 0.01ppp and 0.075ppp respectively. The x- axis is divided into 60 equally spaced bins and the y-axis denotes the number of measurements falling within each bin as a fraction of total number of points. The root mean squared (RMS) error is defined as:

$$RMS\ error = \sqrt{\frac{1}{N} \sum_{i=1}^N e_{i_w}^2} \quad (12)$$

The error distribution for the lower seeding density is sharper with RMS error of about 0.1 pixels compared to RMS error of 0.29 pixels for the higher seeding density case. The predicted uncertainty distributions have significantly less spread and have a tight distribution around the RMS error. For a successful prediction, it is expected that the RMS value of the error distribution should match the RMS value of the estimated uncertainty distribution (Sciacchitano *et al.* 2015). The RMS value for each distribution is indicated by the dashed vertical line. For Figure 3, the RMS uncertainty values are within 0.06 pixels of the RMS error values and are in close agreement, indicating a successful prediction for position reconstruction uncertainty.

Reconstructed position uncertainty for varying particle concentration

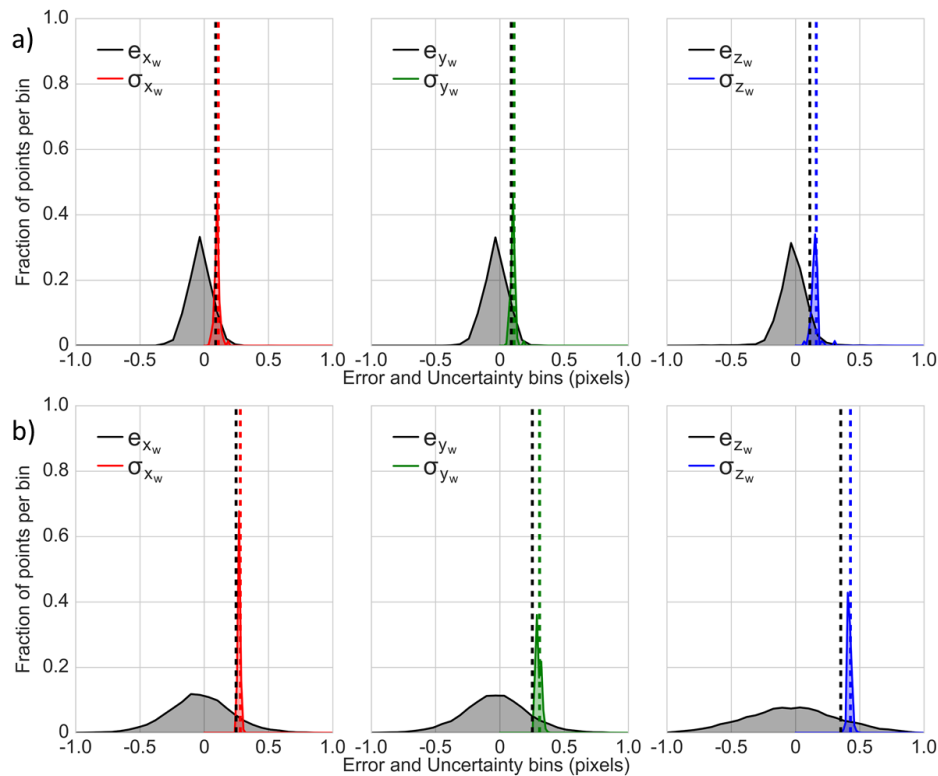


Figure 3: Histogram of error (e) and uncertainty (σ) distributions for reconstructed particle positions (x_w, y_w, z_w) for the synthetic vortex ring case with seeding densities a) 0.01ppp and b) 0.075ppp. The vertical lines indicate the RMS value for each distribution.

The increase in particle concentration leads to a higher percentage of “ghost” particles and eventually increases the error in reconstruction. To test the sensitivity of the uncertainty predictions in such scenarios, the seeding density is varied from 0.01ppp to 0.1ppp and the RMS error and uncertainty values are compared in each case, as shown in Figure 4.

The results show a high sensitivity of the predicted uncertainty to the trend of the RMS error. For a seeding density of 0.01ppp and 0.1ppp, the predicted uncertainty best matches the expected RMS error value. However, it overpredicts for other seeding densities, with a maximum overprediction of 0.05 pixels for 0.05ppp case. Overall trend agreement, between the predicted and the expected uncertainty validates the current framework for prediction of uncertainty in reconstructed 3D particle positions.

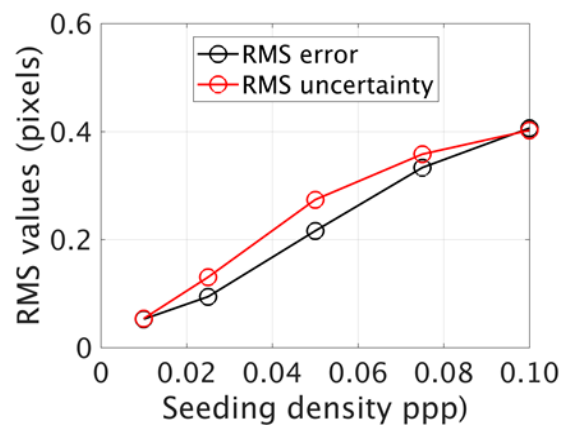


Figure 4: Comparison RMS error and RMS of predicted uncertainties for seeding densities in the range of 0.01ppp to 0.1ppp for the synthetic vortex ring case.

Uncertainty prediction for tracked velocity vectors

As a final step, the uncertainty prediction in the tracked velocity field is assessed. The reconstructed 3D particle positions are tracked for a pair of frames for 10 pairs using nearest-neighbor tracking. The true particle positions in 1 voxel vicinity of the reconstructed particle positions is found for the first frame and the corresponding true displacement is subtracted from the estimated displacement to compute the error (e) in u , v and w velocity components. A measurement is considered valid if the computed error magnitude is within 1 voxel. The uncertainty ($\sigma_u, \sigma_v, \sigma_w$) in the velocity components are computed using equation (10).

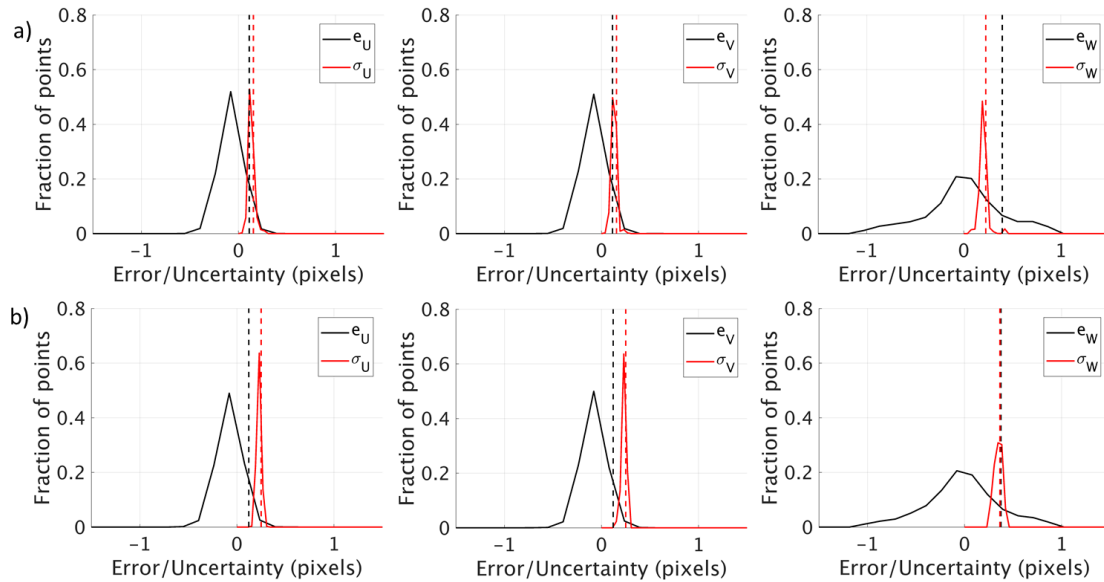


Figure 5: Error and uncertainty histogram comparison for tracked velocity vectors in the synthetic vortex ring case with seeding densities a) 0.01ppp and b) 0.025ppp.

Figure 5a and Figure 5b shows the comparison between the estimated velocity error and uncertainty histogram for 0.01ppp and 0.025ppp seeding density cases respectively. It is noticed that the w component has higher error compared to u and v components. For the lower seeding density case, the uncertainty distributions are sharply distributed within 0.05 pixels of the expected uncertainty value for u and v component, and underpredicts the RMS error by 0.17 pixels for the w component of the displacement. In Figure 5b, the u and v component uncertainty is overestimated by 0.13 pixels, while the predicted uncertainty for the w component exactly matches RMS error value. Further analysis for higher seeding densities with STB processing is required to validate the displacement uncertainty model proposed by equation (10), however, preliminary results show reasonable agreements between predicted and expected uncertainty values for the estimated velocity components.

Experimental Validation: Uncertainty prediction for laminar pipe flow

The current framework is also validated for a canonical laminar pipe flow experiment for a Reynolds number of 600. Four phantom Miro341 cameras set up was used to observe the flow through a 0.25" PTFE tube immersed in a water tank with refractive index matching. The flow was driven in a loop using a gear pump and the flow rate downstream of the test section was measured using an ultrasonic flowmeter with 1% standard deviation. Time-resolved particle images were

captured at 6000Hz framerate(640x624 pixels resolution) for a working volume of 9mmx6.5mmx6.5mm with an average magnification of 17.8 microns/pixel. The expected true velocity profile U_{true} with a standard uncertainty ($\pm\sigma$) due to flow rate measurement is shown in Figure 6. 100 frames were processed with in-house codes using a triangulation reconstruction and 3D nearest neighbor tracking and the current uncertainty propagation model was used to evaluate the uncertainty in the final tracked velocity estimates. A thin horizontal slice of volume (6mmx6mmx1mm) along the center of the pipe is considered and is subdivided along the depth (direction normal to the camera) into 20 bins. The average velocity of the measurements falling in each of those bins is plotted as \bar{U} in Figure 6a. The corresponding standard deviation of measurements within each bin is also shown as the gray shaded region. The estimated velocity profile has a maximum deviation of 0.12 voxels/frame compared to the true velocity. Also, this specific experimental case had higher uncertainty on the mean velocity near the pipe wall at $z = -6mm$. Overall, the mean velocity profile agreed with the expected parabolic profile of a laminar pipe flow.

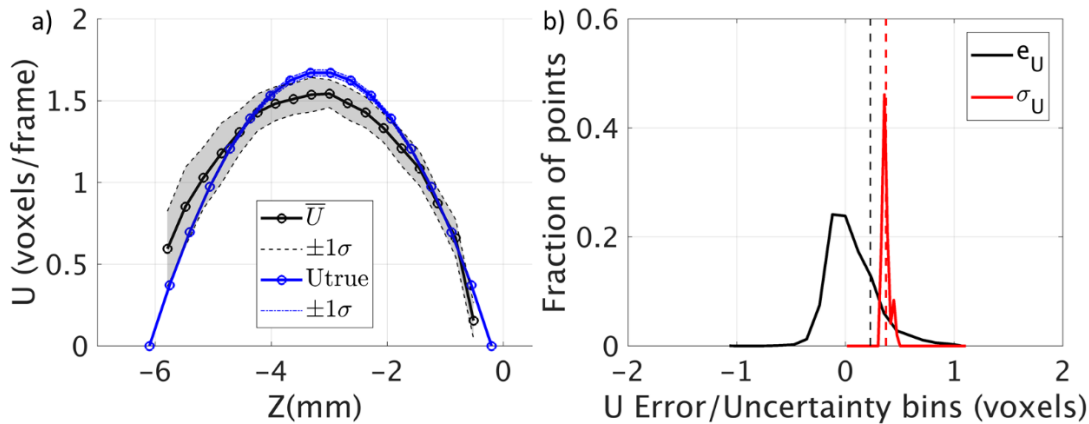


Figure 6: The mean velocity profile for a 3D PTV measurement of a laminar pipe flow is compared with the true solution in a). The corresponding U velocity error and estimated uncertainty distributions are compared in b).

The measured U component of velocity for the points measured in the thin horizontal volume is compared to the true expected velocity and the distribution of error e_U is shown in Figure 6b. The error distribution is skewed with the RMS of error at 0.23 voxels, as depicted by the vertical dashed black line in Figure 6b. The predicted uncertainty σ_U distribution has a shallow spread and has an RMS value of 0.37 voxels. Thus, the predicted uncertainty using current framework shows 0.14 pixels overprediction. However, a better processing using STB method can reduce the error distribution as well as processing higher number of frames, which can improve the statistical convergence.

4 Conclusion

We proposed a comprehensive framework to predict the uncertainty in the reconstructed 3D particle positions in a volumetric PTV measurement and subsequently propagate the uncertainty in the tracked velocity estimates. The variance estimated from the histogram of the reprojection error

provides the uncertainty bound on the particle image position and contributes to the uncertainty in the mapping function coefficients. The uncertainty in the reconstructed particle position directly affects the uncertainty in the displacement estimate. Analysis with the synthetic vortex ring images showed good agreement between the RMS of the predicted uncertainties in x, y, z positions and the RMS error. However, for the uncertainty in the displacement estimates, the prediction was about 0.15 voxels higher for both the vortex ring case and the experimental pipe flow case. Overall, the predicted uncertainties are sharply distributed close to the RMS error values and showed strong sensitivity to the variation in RMS error, even for different seeding densities. Hence, the preliminary results establish the current methodology as a successful predictor for uncertainty in a 3D PTV measurement.

References

- Baek, S. J., & Lee, S. J. (1996). A new two-frame particle tracking algorithm using matching possibility. *Experiments in Fluids*, **22**, 261–304.
- Bhattacharya, S., Charonko, J. J., & Vlachos, P. P. (2017). Stereo-particle image velocimetry uncertainty quantification. *Measurement Science and Technology*, **28**(1), 015301.
- Bhattacharya, S., Charonko, J. J., & Vlachos, P. P. (2018). Particle image velocimetry (PIV) uncertainty quantification using moment of correlation (MC) plane. *Measurement Science and Technology*, **29**(11), 115301.
- Boomsma, A., Bhattacharya, S., Troolin, D., Pothos, S., & Vlachos, P. (2016). A comparative experimental evaluation of uncertainty estimation methods for two-component PIV. *Measurement Science and Technology*, **27**(9), 094006.
- Cardwell, N. D., Vlachos, P. P., & Thole, K. A. (2011). A multi-parametric particle-pairing algorithm for particle tracking in single and multiphase flows. *Measurement Science and Technology*, **22**(10), 105406.
- Charonko, J. J., & Vlachos, P. P. (2013). Estimation of uncertainty bounds for individual particle image velocimetry measurements from cross-correlation peak ratio. *Measurement Science and Technology*, **24**(6), 065301.
- Cowen, E. A., Monismith, S. G., Cowen, E. A., & Monismith, S. G. (1997). A hybrid digital particle tracking velocimetry technique. *Experiments in Fluids*, **22**(3), 199–211.
- Elsinga, G. E., Scarano, F., Wieneke, B., & van Oudheusden, B. W. (2006). Tomographic particle image velocimetry. *Experiments in Fluids*, **41**(6), 933–947.
- Fuchs, T., Hain, R., & Kähler, C. J. (2016). Double-frame 3D-PTV using a tomographic predictor. *Experiments in Fluids*, **57**(11), 174.
- Fuchs, T., Hain, R., & Kähler, C. J. (2017). Non-iterative double-frame 2D/3D particle tracking velocimetry. *Experiments in Fluids*, **58**(9), 119.
- Lei, Y.-C., Tien, W.-H., Duncan, J., ... Hove, J. (2012). A vision-based hybrid particle tracking velocimetry (PTV) technique using a modified cascade correlation peak-finding method. *Experiments in Fluids*, **53**(5), 1251–1268.
- Maas, H. G., Gruen, A., & Papantoniou, D. (1993). Particle tracking velocimetry in three-dimensional flows. *Experiments in Fluids*, **15**(2), 133–146.
- Ohmi, K., & Li, H.-Y. (2000). Particle-tracking velocimetry with new algorithms. *Measurement Science*

and Technology, **11**(6), 603–616.

- Pereira, F., Stüer, H., Graff, E. C., & Gharib, M. (2006). Two-frame 3D particle tracking. *Measurement Science and Technology*, **17**(7), 1680–1692.
- Riethmuller, A. S. and M. L. (2001). Extension of PIV to super resolution using PTV. *Measurement Science and Technology*, **12**(9), 1398.
- Schanz, D., Gesemann, S., & Schröder, A. (2016). Shake-The-Box: Lagrangian particle tracking at high particle image densities. *Experiments in Fluids*, **57**(5), 70.
- Schanz, D., Gesemann, S., Schröder, A., Wieneke, B., & Novara, M. (2013). Non-uniform optical transfer functions in particle imaging: calibration and application to tomographic reconstruction. *Measurement Science and Technology*, **24**(2), 024009.
- Sciacchitano, A. (2019). Uncertainty quantification in particle image velocimetry. *Measurement Science and Technology*. doi:10.1088/1361-6501/ab1db8
- Sciacchitano, A., Neal, D. R., Smith, B. L., ... Scarano, F. (2015). Collaborative framework for PIV uncertainty quantification: comparative assessment of methods. *Measurement Science and Technology*, **26**(7), 074004.
- Sciacchitano, A., Wieneke, B., & Scarano, F. (2013). PIV uncertainty quantification by image matching. *Measurement Science and Technology*, **24**(4), 045302.
- Soloff, S. M., Adrian, R. J., & Liu, Z. C. (1997). Distortion compensation for generalized stereoscopic particle image velocimetry. *Measurement Science & Technology*, **8**(12), 1441–1454.
- Takehara, K., Adrian, R. J., Etoh, G. T., & Christensen, K. T. (2000). A Kalman tracker for super-resolution PIV. *Experiments in Fluids*, **29**(1), S034–S041.
- Timmins, B. H., Wilson, B. W., Smith, B. L., & Vlachos, P. P. (2012). A method for automatic estimation of instantaneous local uncertainty in particle image velocimetry measurements. *Experiments in Fluids*. doi:10.1007/s00348-012-1341-1
- Wieneke, B. (2008). Volume self-calibration for 3D particle image velocimetry. *Experiments in Fluids*, **45**, 549–556.
- Wieneke, B. (2013). Iterative reconstruction of volumetric particle distribution. *Measurement Science and Technology*, **24**(2), 024008.
- Wieneke, B. (2015). PIV uncertainty quantification from correlation statistics. *Measurement Science and Technology*, **26**(7), 074002.
- Wu, J.-Z., Ma, H.-Y., & Zhou, M.-D. (2006). *Vorticity and Vortex Dynamics*, Berlin, Heidelberg: Springer Berlin Heidelberg. doi:10.1007/978-3-540-29028-5
- Xue, Z., Charonko, J. J., & Vlachos, P. P. (2014). Particle image velocimetry correlation signal-to-noise ratio metrics and measurement uncertainty quantification. *Measurement Science and Technology*, **25**(11), 115301, Fluid Dynamics.
- Xue, Z., Charonko, J. J., & Vlachos, P. P. (2015). Particle image pattern mutual information and uncertainty estimation for particle image velocimetry. *Measurement Science and Technology*, **26**(7), 074001.